AGU PUBLICATIONS

JGR

Journal of Geophysical Research: Earth Surface

RESEARCH ARTICLE

10.1002/2014JF003183

Key Points:
- Process-transformation makes rock-ice avalanches different from rock avalanches
- Two-phase mechanical model for dynamic strength weakening enhances flow mobility
- Internal mass and momentum exchange generate frontal surge head and secondary surges

Correspondence to:
S. P. Pudasaini,
pudasaini@geo.uni-bonn.de

Citation:
Pudasaini, S. P., and M. Krautblatter (2014), A two-phase mechanical model for rock-ice avalanches, *J. Geophys. Res. Earth Surf.*, *119*, doi:10.1002/2014JF003183.

Received 17 APR 2014
Accepted 17 SEP 2014
Accepted article online 19 SEP 2014

A two-phase mechanical model for rock-ice avalanches

Shiva P. Pudasaini[1] and Michael Krautblatter[2]

[1]Department of Geodynamics and Geophysics, Steinmann Institute, University of Bonn, Bonn, Germany, [2]Landslide Research, Faculty of Civil, Geo and Environmental Engineering, Technical University Munich, Munich, Germany

Abstract Rock-ice avalanche events are among the most hazardous natural disasters in the last century. In contrast to rock avalanches, the solid phase (ice) can transform to fluid during the course of the rock-ice avalanche and fundamentally alter mechanical processes. A real two-phase debris flow model could better address the dynamic interaction of solid (rock and ice) and fluid (water, snow, slurry, and fine particles) than presently used single-phase Voellmy- or Coulomb-type models. We present a two-phase model capable of performing dynamic strength weakening due to internal fluidization and basal lubrication and internal mass and momentum exchanges between the phases. Effective basal and internal friction angles are variable and correspond to evolving effective solid volume fraction, friction factors, volume fraction of the ice, true friction coefficients, and lubrication and fluidization factors. Benchmark numerical simulations demonstrate that the two-phase model can explain dynamically changing frictional properties of rock-ice avalanches that occur internally and along the flow path. The interphase mass and momentum exchanges are capable of demonstrating the mechanics of frontal surge head and multiple other surges in the debris body. This is an observed phenomenon in a real two-phase debris flow, but newly simulated here by applying the two-phase mass flow model. Mass and momentum exchanges between the phases and the associated internal and basal strength weakening control the exceptional long runout distances, provide a more realistic simulation especially during the critical initial and propagation stages of avalanche, and explain the exceptionally high and dynamically changing mobility of rock-ice avalanches.

1. Introduction

Rock-ice avalanches occur in permafrost-affected or glaciarized high mountain environments. These regions are increasingly threatened by high-magnitude low-frequency rock-ice avalanches [*Evans and Clague*, 1988, 1998, *Hewitt*, 1999, 2008; *Margreth and Funk*, 1999; *Deline*, 2001; *Giani et al.*, 2001; *McSaveney*, 2002; *Huggel et al.*, 2005, 2007, 2008; *Kääb et al.*, 2005; *Korup*, 2005; *Schneider*, 2006; *Lipovsky et al.*, 2008; *Sosio et al.*, 2008; *Schneider et al.*, 2010]. In the context of changing climate, growing population pressure, increasing infrastructural development, and recreational activities, rock-ice avalanches increasingly put humans and infrastructure at risk [*Haeberli et al.*, 1997; *Schneider et al.*, 2010; *Sosio et al.*, 2012; *Krautblatter et al.*, 2013]. As flows and deposition volumes can exceed 10^9 m^3 and can reach speeds of 100 m s^{-1}, sometimes travelling 10 s of kilometers, rock-ice avalanches pose serious risks and cause catastrophic damage when they reach populated regions.

Different types of rock flows are among the most catastrophic mass movements described by their large volumes, spreading, devastating consequences and costs [*Crosta et al.*, 2004; *Hungr*, 2004; *Evans*, 2006; *Geertsema et al.*, 2006; *Pudasaini and Hutter*, 2007; *Sosio et al.*, 2008; *Pirulli*, 2009; *Pudasaini and Miller*, 2013]. In the last decades, a number of exceptional rock slope failures occurred in the Caucasus, the European Alps, and Alaska [*Sosio et al.*, 2008; *Huggel*, 2009; *Pirulli*, 2009]. Climatically and hydrologically driven permafrost degradation, thermal perturbations, heat conduction, and advection in active and deep layers may have triggered many of the recent rockfalls in high-Alpine steep rockwalls [*Schiermeier*, 2003; *Gruber et al.*, 2004; *Gruber and Haeberli*, 2007; *Huggel*, 2009; *Ravanel and Deline*, 2011]. Huge rock-ice masses detached in Huascaran (Peru, 1962, 1970) caused thousands of casualties [*Plafker and Ericksen*, 1978; *Körner*, 1983; *Evans et al.*, 2009a; *Schneider et al.*, 2010]. Another extremely mobile and catastrophic rock-ice avalanche occurred in 2002 in Kolka glacier, Russian Caucasus with 120 casualties [*Haeberli et al.*, 2004; *Kotlyakov et al.*, 2004; *Huggel et al.*, 2005; *Evans et al.*, 2009b; *Schneider et al.*, 2011a].

Especially the Huascaran and the Kolka Karmadon events highlight a mechanical and a flow dynamical point of view for rock-ice avalanche. These events consisted of rock, ice, snow, and water. High ice contents, flow

transformations to debris flows, exceptionally long travel distances (hypermobility, [*Pudasaini and Miller*, 2013]), and very high velocities characterize these events due to both the moving material and the material of the sliding path consisting of the exposed rock beds, glacial deposits, glacier, and vegetation [*Petrakov et al.*, 2008; *Schneider et al.*, 2011a]. Most often these flows block major rivers and create artificial dams [*Strom and Korup*, 2006; *Hewitt et al.*, 2008]. Considerable attention has been drawn in the past to investigate the mechanism of slope failure, material properties, physical modeling of the flow and their numerical simulations, geomorphological characteristics, debris impact, and mitigation strategies related to rock-ice avalanches [*Govi*, 1989; *Huber*, 1992; *Dramis et al.*, 1995; *Crosta et al.*, 2004; *Sosio et al.*, 2008; *Pirulli*, 2009].

Rock-ice avalanche events are more challenging than the other types of mass flows [*Schneider et al.*, 2010]. First, they consist of materials with different physical and rheological properties (rock, ice, snow, fluid, etc.), and second, during the propagation they show changing flow behavior as the snow and ice melts by frictional heating producing sufficient fluid, or incorporation of water that transforms the initial rock avalanche into a rock-ice-fluid debris flows. The laboratory and field observations clearly reveal changing flow properties from solid-like to fluid-like and thus largely showing the two-phase nature of the flow as the rock-ice mass propagates downslope. This could be the main reason that none of the available models are able to simulate these complex events with process transformations and interactions by simply using over simplified, and effectively single-phase mass flow models which were basically developed to simulate single-phase granular flows, such as dry snow and rock avalanches [*Hungr and Evans*, 1996; *Bottino et al.*, 2002; *Crosta et al.*, 2004; *Armento et al.*, 2008; *Pirulli and Sorbino*, 2008; *Schneider et al.*, 2010; *Sosio et al.*, 2012]. *Bottino et al.* [2002] used block-fall models to simulate the 1936 Felik landslide and rock-ice avalanches in the Brenva Glacier (Mount Blanc Massif) in 1920 and 1997. Their results show that real runouts exceed predicted ones by 30%. They infer that this might possibly be due to fluidization processes.

Unlike for snow avalanches [*Surinach et al.*, 2000], the unprecedented breaking-off of large rock-ice avalanches implies that any direct physical and field measurements are almost impossible [*Schneider et al.*, 2011a]. Field data are limited, and laboratory measurements mainly provide wide spectrum of flow mechanical information in a steady-state controlled laboratory rock-ice avalanches [*Schneider et al.*, 2011a]. However, the full understanding of the process dynamics requires the complete simulation of the event from initiation to the depositions. Numerical simulations of rock-ice avalanches based on continuum mechanical models provide deterministic evolution of the flow velocity, flow depth, and total runout distances and can predict the extent of the potential impact area, destructive impact forces, mechanism of flow mobility, and deposition characteristics. This is necessary for the appropriate design of countermeasures and defense structures, the hazard mitigation, risk assessments, and construction of hazard maps [*Chen and Lee*, 2000; *Denlinger and Iverson*, 2001, 2004; *Bottino et al.*, 2002; *McDougall and Hungr*, 2004; *Crosta et al.*, 2004, 2006; *McSaveney and Davies*, 2006; *Chen et al.*, 2006; *Pudasaini and Hutter*, 2007; *Schneider et al.*, 2010; *Sosio et al.*, 2012].

Today, the most widely used and largely successful models for rockslides, rock avalanches, and granular flows are based on the continuum mechanics which are effectively single phase. The basal shear stresses are often closed with a rate-independent Coulomb friction and an empirical Voellmy term for velocity-dependent turbulent resistance [*Voellmy*, 1955; *Savage and Hutter*, 1989; *Denlinger and Iverson*, 2004; *Pudasaini and Hutter*, 2003, 2007; *Crosta et al.*, 2004; *McDougall and Hungr*, 2004; *Pudasaini et al.*, 2005a, 2005b; *Sosio et al.*, 2008; *Pirulli*, 2009; *Bartelt et al.*, 2012; *Fischer et al.*, 2012; *Sosio et al.*, 2012]. To adjust simulation with observation, effective Coulomb and Voellmy parameters are often largely varied from 0.03 to 0.25 and 100 and 1000 [*Crosta et al.*, 2004; *Sosio et al.*, 2008; *Pirulli*, 2009] and relatively low values are often preferred. Similarly, rock-ice avalanches are simulated by using Coulomb friction and Voellmy flow resistances, μ and ξ. The frictional coefficient ranges in the interval from 0.03 to 0.1, the Voellmy coefficient within 1000 m s^{-2} to 6500 m s^{-2} [*Schneider et al.*, 2010]. Some modelers use higher parameter (μ and ξ) values [*Schneider et al.*, 2010] than the others [*Hungr and Evans*, 1996; *Lipovsky et al.*, 2008; *Sosio et al.*, 2008]. Even for the icy basal surfaces these values of μ are very low [*Schneider et al.*, 2010]. It is surprising that the same Coulomb-Voellmy rheology requires different parameter sets for the same events to back calculate them. Systematic constraining of these parameters is somehow unmanageable. The Voellmy model is widely used in application in snow and rock avalanche dynamics. However, somehow its use is still in debate because of the lacking of the physical meaning and verification of the rheological parameters although there were attempts to physically quantify the parameter values [*Schneider et al.*, 2010; *Fischer et al.*, 2012]. Therefore, the large uncertainty in parameter selection may demand for more sophisticated models that

take into account the naturally two-phase nature of the flows consisting of the solid rock particles and ice and the interstitial fluid [*Sosio et al.*, 2012].

Coulomb-Voellmy-type models are based on effectively single-phase dry granular flows in which the fluid effect is only passively incorporated by reducing the dry Coulomb friction. These naturally pose fundamental questions about (i) the applicability of simple and pure (dry) Coulomb friction and Voellmy friction and (ii) the use of single-phase model equations. From the risk assessment and planning point of view, it is important to use appropriate physical-mathematical models and simulation tools to foresee areas hit and covered by materials mobilized during rock-ice avalanches. Although rock-ice avalanches in glacial environments are particularly dangerous, and their modelling and simulation are an emerging field, these events are still very poorly understood [*Hungr and Evans*, 1996; *Bottino et al.*, 2002; *Crosta et al.*, 2004; *Armento et al.*, 2008; *Pirulli and Sorbino*, 2008; *Schneider et al.*, 2010; *Ravanel and Deline*, 2011; *Sosio et al.*, 2012] in terms of dimensions, phases and mechanics. None of the physical models and simulations yet include observed fluidization and lubrication phenomena, enhanced mobility, interphase mass and momentum exchanges, and surge development in rock-ice avalanche.

This paper presents a new mechanically enhanced approach to model and simulate rock-ice avalanches to help to improve our understanding of the complex, inherently two-phase dynamical processes by using physically constrained parameters. This is achieved with a high-resolution computational runout model. Here we present benchmark simulations of rock-ice avalanche dynamics with a real two-phase model. To do so, we consider the general two-phase model equations presented by *Pudasaini* [2012]. We include the additional mechanics and dynamical effects induced by the ice in the rock-ice mass and glacier ice entrainment. Our new modeling concept takes into account: lubrication and fluidization effects, and internal mass and momentum exchanges (between the phases) favored by flow transformation into the debris flows (in terms of the mass and the momentum productions and losses [*Sosio et al.*, 2012]). The outcome is assessed in terms of the front amplification and position, and surges. We demonstrate how the additional physical processes, like interphase mass and momentum exchanges from solid to fluid, lead to novel concepts and results in modeling the two-phase rock-ice avalanches.

2. Mechanics Related to the Dynamics of Rock-Ice Avalanches

Permafrost debris masses consist of the solid (rock and ice) and fluid constituents. Distribution of ice may exert significant influences on the dynamics of the rock-ice avalanches in comparison to the pure rock avalanches. The mobility of a rock-ice avalanche is controlled mainly by the amount of snow and ice available in the moving material and smooth icy basal surfaces. A rock-ice avalanche may consist of up to 90% ice and snow [*Schneider et al.*, 2010; *Sosio et al.*, 2012].

When the detached rock-ice mass strongly impacts the ground and fragments into small pieces, large internal shearing takes place, or if the mass reaches regions with a larger boundary friction, more kinetic energy is dissipated [*Schneider et al.*, 2011a]. Dynamic grain fragmentation [*McSaveney and Davies*, 2007; *Davies et al.*, 2010] and large pressure-induced enhanced melting of the ice are likely to be present in large natural events [*Davies and McSaveney*, 1999]. In these scenarios, as in 2007 Bliggspitze event (Figure 1), quickly a large amount of water may be produced by fragmenting and melting of ice. The moving mass could be fluidized (behave like a fluid with negligible shear strength) through the depth, or the liquid may possibly be concentrated in thin basal shear layers (lubrication), or both. In both situations the flow mobility increases in terms of travel distances and the total inundation area.

Schneider et al. [2011a] have quantified the influence of the ice (between 0 and 100%) and water content on the bulk friction coefficients in laboratory experiments. The flow appeared to be largely dry and granular at the early phase of experiment. But, for laboratory and field events the frictions can further be reduced, and the effective friction coefficient can be as low as 0.11 [*Schneider et al.*, 2011a]. Mixing of the rock particles with ice, snow, and possibly fluid reduces basal friction. The frictional heat induced at the sliding surface results in the melting of ice, which depends on the amount of the ice available in the mixture. This reduces the material friction through the basal saturation, pore pressure generation, or lubrication, and fluidization leading to the enhanced mobility [*Marangunic and Bull*, 1968; *Erismann*, 1979; *Legros et al.*, 2000; *Erismann and Abele*, 2001; *McSaveney*, 2002; *Bartelt et al.*, 2006; *De Blasio and Elverhøi*, 2008; *Sosio et al.*, 2012].

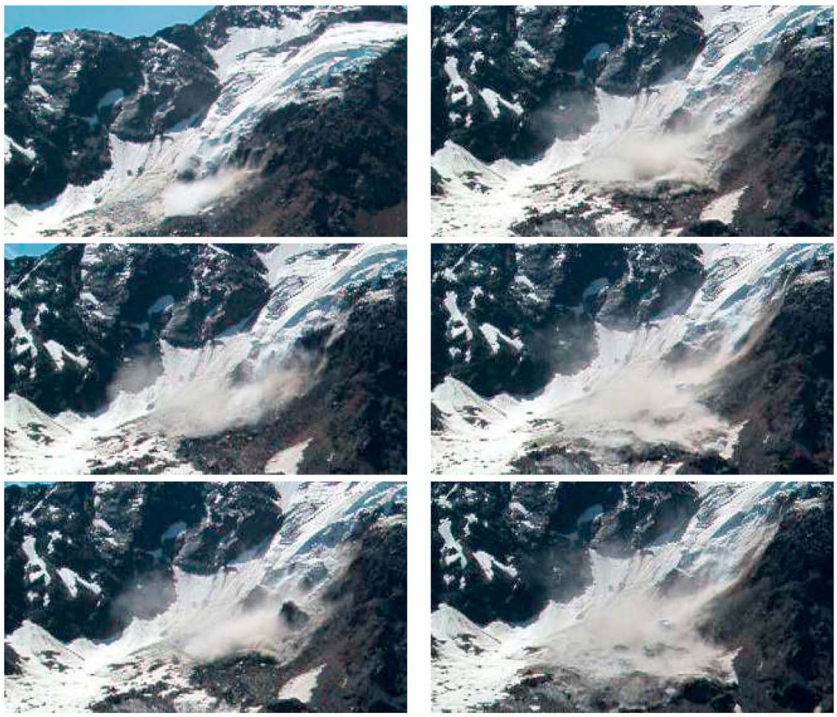

Figure 1. Dynamics of Bliggspitze (2007) rock-ice avalanche. The time sequence, [0.0, 1.0, 1.1, 1.15, 1.22, 1.25] s, where 0.0 is the reference time (from left top to bottom, then right top to bottom) presents the collapse of the rock-ice wall, fluidization, and the debris surge developments. Photo source: Dr. Gunther Heissel.

In the sequel, we briefly discuss the main aspects and mechanisms related to the dynamics of rock-ice avalanches. This includes in situ snow and ice covers, ice, and glaciers; entrainment of ice, water, and sediment; density and effective solid volume fraction; basal lubrication and internal fluidization; flow transformation; and internal mass and momentum exchanges.

2.1. In Situ Snow and Ice Covers, Ice, and Glaciers

Prefailure, ice in permafrost rocks exists inside the bedrock in pores, discontinuities, and cavities [*Draebing and Krautblatter*, 2012] as well as on the rock face as snow, firn and ice cover, and glaciers. Recent events [*Huggel*, 2009] demonstrate that a significant share of this ice may turn into fluid (water) immediately after the rock slope failure, as observed in the field, e.g., at the Bliggspitze (Figure 1). The fluid may penetrate the fragmented rock-ice mass. This will (i) internally reduce the friction between the solid particles (rock and ice), thus fluidizing the mass; (ii) reduce the basal slip as the fluid reaches the basal surface; (iii) induce a buoyancy force, and (iv) rise the fluid pressure.

2.2. Entrainment of Ice, Water, and Sediment

Fluid-related effects are amplified if additional water is supplied by lakes in the starting zone of the rock avalanche or if water from lakes, rivers, and water-saturated sediments is entrained during the flow [*Crosta et al.*, 2004; *Strom and Korup*, 2006; *Hewitt et al.*, 2008; *Schneider et al.*, 2011b]. Lake, river and entrained groundwater, snow cover, and melted ice constitute the fluid component, the main agent of strength weakening, fluidization, lubrication, buoyancy, mass exchanges, mass addition or loss, etc.

2.3. Density and Effective Solid Volume Fraction

The amount and distribution of the ice mass plays a significant role in the rock-ice avalanche dynamics. To realize this, let, ρ_s and ρ_f be the densities of the solid and fluid; and α_r, α_i, and α_f be the volume fractions of the rock, ice, and the fluid. Then, $\alpha_s = \alpha_r + \alpha_i$ is the volume fraction of the solid, and $\alpha_f = 1 - \alpha_s$ for the fluid. The density of the ice (ρ_i) is much lower than the density of the rock (ρ_r); $\rho_r = \lambda_\rho \rho_i$, where λ_ρ is the density factor. So, $\alpha_s\rho_s = \alpha_r\rho_r + \alpha_i\rho_i = \rho_r[\alpha_r + \alpha_i/\lambda_\rho] = \rho_r\alpha_s^e$ is the effective solid mass. The total solid contribution $\alpha_s\rho_s = \rho_r\alpha_s^e$ is expressed in terms of the rock density and the effective solid volume fraction α_s^e, where $\alpha_r \leq \alpha_s^e \leq 1$; α_s^e, which represents the rock and ice volume fraction distribution together, emerged as the new field variable. We discuss in detail in section 3 on how α_s^e effects the dynamics of two-phase flow.

2.4. Basal Lubrication and Internal Fluidization

The accurate knowledge of the basal and internal friction parameters is necessary as they mechanically control the basal shear stress, internal deformation, anisotropy of the stresses (through the earth pressure coefficient), and hydraulic pressure gradient of the solid constituent. In large rock avalanches associated with high pressure (normal load), the frictional heat at the sliding plane causes temperature rise in rare cases to more than 1000 K [*Pudasaini and Hutter*, 2007]. In rock-ice avalanches, ice (and rock gravels) melts and the molten ice (and rock) liquid lubricates the sliding surface which has not been considered yet in simulation. Since the mass is composed of (dry) rock and ice, the ice will melt relatively quickly forming a thin lubricating water (or slurry) film at the sliding base. In turn, this will heavily reduce basal friction, economize the flow (both at the base and internally if the mass is fluidized or sheared).

Rock-ice avalanches that propagate onto icy surfaces, or glaciers often exhibit exceptionally enhanced mobility. This is usually explained by three mechanisms [*McSaveney*, 1978; *Plafker and Ericksen*, 1978; *Evans and Clague*, 1988; *Geertsema et al.*, 2006; *Evans et al.*, 2009a]. (1) Reducing the friction and inducing fluidization within the propagating mass due to the presence of ice, snow, and fluid in the moving mass. This eventually transforms the initially solid-like dry rock avalanches into a fluid-like debris flows (Figure 1). (2) Frictional heating or compression of snow along the glacier elevates the basal fluid saturation. As the ice melts due to frictional heating pore pressure increases. This consequently reduces the shear resistance of the flowing material. (3) Reduced friction at the debris-glacier interface. It is estimated that these factors can result in more than 25% higher mobility of rock-ice avalanches [*Evans and Clague*, 1988; *Huggel et al.*, 2005].

Schneider et al. [2011a] verified the first two mechanisms with laboratory experiments carried out in rotating drums partially filled with the mixture of gravel and gravel-sized ice particles. They reveal many fundamental mechanical aspects of rock-ice mass flows, e.g., the decrease of bulk friction with increasing ice content. However, this reduction in the bulk friction angle can approach 50%. For ice contents larger than 40%, the moving mass transforms from a dry granular flow into a fluidized debris flow.

Here, based on observations (Bliggspitze, 2007, Austria; Mount Rainier, 2011, USA [*Sosio et al.*, 2012; *Schneider et al.*, 2011a]), we propose three mechanisms that result in enhanced mobility of the rock-ice avalanche. (4) As the ice and snow melts during the propagation [*Schneider et al.*, 2011a], the material strength reduces internally and along the basal surface due to the reduction of the internal and basal frictions leading to the internal fluidization and basal lubrication. This requires mechanical models that dynamically describe the fluidization and lubrication effects. (5) The propagating mass quickly transforms from an initial solid-like single-phase rock avalanche into a two-phase solid-fluid mixture debris flow, or even debris flood and hyperconcentrated flows [*Schneider et al.*, 2011a]. (6) As the ice and snow contained in the moving mass melt, more and more solid (say, ice) mass transforms into fluid from the initially rock-ice material. This highlights the importance of the internal mass and momentum exchanges between the solid and fluid phases. This is a very special phenomenon observed in the rock-ice avalanche (Figure 1 and *Schneider et al.* [2011a]) that is generally not present in other types of geophysical mass flows. Although (4) is somehow an extension of (1) and (2) and unifies several aspects, (5) and (6) are new insights in modeling and simulation of rock-ice avalanches. Points (4)–(6) can further be extended to include (3) and the basal entrainment and deposition processes. So, classically widely used effectively single-phase mass flow models based on the description of dry granular flows with Coulomb, and Voellmy rheology that relies on the empirical fit parameters cannot fully address issues (4)–(6).

2.5. Flow Transformation

Rock avalanches overlain by a dusty cloud of fragmented rocks and ice, and meltwater may transform the rock avalanche into a muddy dense flow in just a couple of seconds during collapse and propagation of rock-ice avalanches as observed by video recording of the 2007 Bliggspitze, and the 2011 Mount Rainier events [*Sosio et al.*, 2012]. In natural debris flows, the dry fronts are often followed by a more liquid body and long tail [*Major and Iverson*, 1999; *Iverson and Denlinger*, 2001; *Pudasaini et al.*, 2005b; *McArdell et al.*, 2007; *Pudasaini*, 2012]. The drum experiments by *Schneider et al.* [2011a] also show that the pore water pressure evolves from the back to the front. However, it also saturates the front when enough meltwater is available to saturate the leading front head. In this situation, the flow transforms into a debris flood or hyperconcentrated flow [*Pierson and Scott*, 1985]. This is also observed visually in the recorded 2007 Bliggspitze event (Figure 1).

2.6. Mass and Momentum Exchanges

During collapse, impact at the ground, deformation, and flow, some ice is converted into fluid (water). Fractions of the solid mass would be transformed to fluid mass. If the mass exchange (migration) between (from) the solid and (to) the fluid is substantial, then mass and momentum balances must be enhanced with some suitable mass and momentum production models. From the mass point of view, the solid momentum is lost and the fluid momentum is gained. Since the solid phase follows the Coulomb-type frictional law, the shear heating is proportional to the shear stress which is proportional to the normal load [*Sosio et al.*, 2012]. It is legitimate to assume that the mass exchange between the ice and the fluid is proportional to the actual solid normal load of the ice, which is a fraction of the effective (actual) solid normal load. The momentum exchanges between the solid and the fluid phases are modeled similarly. This is explained in section 3.2.

3. A Two-Phase Dynamical Model for Rock-Ice Avalanche

3.1. Modeling Basal Lubrication and Internal Fluidization

Here we develop a new rheological model to describe the evolution of the effective basal and internal friction angles in terms of the effective solid volume fraction, friction factors, volume fraction of the ice, true friction coefficients; and basal lubrication and internal fluidization factors that are functions of several physical parameters and mechanical/dynamical variables, including the volume fractions of the solid, shear rate and the normal stresses. Thus, the effective internal and basal friction angles are no more constant for rock-ice-avalanche, as they classically are [*Crosta et al.*, 2004; *Sosio et al.*, 2008, 2012; *Pirulli*, 2009; *Schneider et al.*, 2011b], but they in fact are functions of the evolving effective solid volume fraction, a field variable in our dynamical model equations. This fundamentally influences the overall dynamics and leads to more rapid flows with large runout distances, distinct depositional morphology as compared to dry rock avalanches.

The presence of ice modifies the effective internal (ϕ_s^e) and basal (δ_s^e) friction angles of the solid constituent, here rock and ice. Let (ϕ_r, δ_r) and (ϕ_i, δ_i) be the friction angles for the rock and ice materials, respectively. Also, let $F_\phi = F_\phi(\alpha_f, \alpha_i, \dot{\gamma}, N, \ldots)$ and $L_\delta = L_\delta(\alpha_f, \alpha_i, \dot{\gamma}, N, \ldots)$ be the fluidization and lubrication factors, where $\dot{\gamma}$ is the shear rate and N is the normal load. Then, the effective internal and basal friction angles can be expressed by the weighted means with respect to the volume fractions which is then enhanced by the fluidization and lubrication factors, respectively:

$$\phi_s^e = \left[\frac{\alpha_r\phi_r + \alpha_i\phi_i}{\alpha_r + \alpha_i}\right] F_\phi = \left[\frac{1}{\alpha_s}\left(\alpha_r\phi_r + \alpha_i\phi_i\right)\right] F_\phi, \quad \delta_s^e = \left[\frac{\alpha_r\delta_r + \alpha_i\delta_i}{\alpha_r + \alpha_i}\right] L_\delta = \left[\frac{1}{\alpha_s}\left(\alpha_r\delta_r + \alpha_i\delta_i\right)\right] L_\delta. \tag{1}$$

Equation (1) recovers the internal and basal friction angles of the rock and ice in the absence of another. This equation can be cast in terms of the new field variable α_s^e, the effective solid volume fraction (section 2.3). The internal and basal frictions of the rock and ice can be related by some measurable positive friction factors λ_ϕ and λ_δ (much less than unity) such that $\phi_i = \lambda_\phi\phi_r$ and $\delta_i = \lambda_\delta\delta_r$. Then, by assuming the density ratio between the rock and ice to be 3 ($\lambda_\rho = 2.7/0.9$, subject to change) and with the definition $\alpha_s^e = \alpha_r + \alpha_i/\lambda_\rho$, see section 2.3, (1) becomes the following:

$$\phi_s^e = \left[\frac{\alpha_s^e + (3\lambda_\phi - 1)\alpha_i/3}{\alpha_s^e + 2\alpha_i/3}\right] \phi_r F_\phi, \quad \delta_s^e = \left[\frac{\alpha_s^e + (3\lambda_\delta - 1)\alpha_i/3}{\alpha_s^e + 2\alpha_i/3}\right] \delta_r L_\delta, \tag{2}$$

where 2/3 corresponds to the factor $(1 - 1/\lambda_\rho)$ that emerges in the derivation of (2). Generally, ϕ_s^e and δ_s^e are decreasing functions of α_s^e. Typically, α_i is a decreasing function of time and space and can be constrained [*Schneider et al.*, 2011a].

The advantage of (2) is that now the effective internal and the basal friction angle are expressed in terms of the known internal and the basal friction angles of the rock (δ_r and ϕ_r), the evolving new field variable α_s^e associated with the effective solid volume fraction, and the fluidization and lubrication factors (F_ϕ and L_δ). Parameterizations or closures are still needed for F_ϕ and L_δ. However, we can constrain them while calibrating the model simulation with the field events or data. Furthermore, if α_i is substantially smaller than α_s^e, then the terms associated with α_i can be neglected. In this case, (2) simply reduce to $\phi_s^e = \phi_r F_\phi$, $\delta_s^e = \delta_r L_\delta$, suggesting that the positive factors F_ϕ and L_δ can at most be unity. Values of F_ϕ and L_δ close to zero indicate hypermobility [*Pudasaini and Miller*, 2013].

3.2. Modeling Internal Mass and Momentum Productions/Exchanges

The interphase mass and momentum exchanges can be introduced with suitable exchange rates, such that, as time evolves and the material moves down, internally certain amount of the solid mass is transformed into fluid [*Schneider et al.*, 2011a]. Similarly, interphase momentum exchanges can be modeled by multiplying the mass exchanges by relevant phase velocities. *Sosio et al.* [2012] estimated the melting efficiency for the Sherman landslide. The thickness of the melted ice, h_{i_m}, was estimated as $h_{i_m} = e\frac{\tau u}{Q\rho_i}$, where $e \in [0, 1]$ is the thermodynamic parameter that indicates that only a certain amount of produced heat is dissipated resulting in ice melting; $\tau = \rho gh\cos\zeta \tan\delta_s^e$ is the basal Coulomb frictional resistance in which ρ and δ_s^e are the effective density and the effective basal friction of the moving bulk as given by (2). Similarly, h and u are the thickness and velocity of the bulk debris, ζ is the slope angle, Q is the latent heat of the ice and ρ_i is the ice density. The values of these parameters as provided in *Sosio et al.* [2012] are $Q = 333.5$ kJ m^{-3}, $\rho_i = 907$ kg m^{-3}, $\rho = 1500$ kg m^{-3}, $e \in [0.3, 0.7]$. Other parameters (functions), e.g., δ_s^e are dynamically calculated from our model (2). In *Sosio et al.* [2012], mass production rate is mainly based on the bulk velocity which we advance here by replacing the bulk velocity by the representative mixture velocity (also called the fluidization velocity) $u_m = u_s\alpha_s^e + u_f\alpha_f$ in h_{i_m}, where u_s and u_f are the solid- and fluid-phase velocities. So, as the thickness of the melted ice is a function of the velocity and the depth of the rock-ice bulk [*Sosio et al.*, 2012], we model the mass production rate M_{pf} (loss in the solid mass and production in the fluid mass) for fluid as a function of $\alpha_s^e h u_m$, where $\alpha_s^e h$ is the "effective solid mass." The required production rate is then obtained by multiplying this with the factor M_{pf}, which collectively contains all the parameters involved in h_{i_m} other than $\alpha_s^e h u_m$. So, the numerical value of M_{pf} is determined by the geometrical and physical parameters such as the slope, effective friction angles, and bulk density.

The mass exchange is proportional to the actual solid mass that consists of the rock and the ice masses; in a simple situation, the mass gain for fluid ($\mathcal{M}_p$) can be modeled by $\mathcal{M}_p = M_{pf}\alpha_s^e h u_m$. The momentum loss in solid and gain in fluid are accordingly introduced (section 3.3). The interphasial momentum exchange is likely to be crucial for modeling of the complex evolution of the form of the debris mass, such as the amplification and superelevation of the debris front and thinning in the tail side and the multiple surges in between.

3.3. The New Model

We consider the general two-phase debris flow model [*Pudasaini*, 2012] and reduce it to one-dimensional inclined channel flow [*Pudasaini and Miller*, 2012a, 2012b; *Pudasaini*, 2014]. Then, with the above introduced mechanical models, variables, and parameters, the new dynamical model for rock-ice avalanche consists of the depth-averaged mass and momentum conservation equations for the effective solid and the fluid phases as follows:

$$\frac{\partial}{\partial t}\left(\alpha_s^e h\right) + \frac{\partial}{\partial x}\left(\alpha_s^e h u_s\right) = -\mathcal{M}_p, \quad \frac{\partial}{\partial t}\left(\alpha_f h\right) + \frac{\partial}{\partial x}\left(\alpha_f h u_f\right) = \mathcal{M}_p, \tag{3}$$

$$\begin{aligned} \frac{\partial}{\partial t}\left[\alpha_s^e h\left(u_s - \gamma C\left(u_f - u_s\right)\right)\right] + \frac{\partial}{\partial x}\left[\alpha_s^e h\left(u_s^2 - \gamma C\left(u_f^2 - u_s^2\right) + \beta_s\frac{h}{2}\right)\right] &= hS_s - \mathcal{M}_p u_s, \\ \frac{\partial}{\partial t}\left[\alpha_f h\left(u_f + \frac{\alpha_s^e}{\alpha_f} C\left(u_f - u_s\right)\right)\right] + \frac{\partial}{\partial x}\left[\alpha_f h\left(u_f^2 + \frac{\alpha_s^e}{\alpha_f} C\left(u_f^2 - u_s^2\right) + \beta_f\frac{h}{2}\right)\right] &= hS_f + \frac{1}{\gamma}\mathcal{M}_p u_f, \end{aligned} \tag{4}$$

where the source terms are given by the following:

$$S_s = \alpha_s^e\left[g^x - \frac{u_s}{|u_s|}\tan\delta_s^e p_{b_s} - \varepsilon p_{b_s}\frac{\partial b}{\partial x}\right] - \varepsilon\alpha_s^e\gamma p_{b_f}\left[\frac{\partial h}{\partial x} + \frac{\partial b}{\partial x}\right] + C_{DG}\left(u_f - u_s\right)|u_f - u_s|^{j-1}, \tag{5}$$

$$\begin{aligned} S_f = \alpha_f\Bigg[g^x - \varepsilon\Bigg[\frac{1}{2}p_{b_f}\frac{h}{\alpha_f}\frac{\partial\alpha_s^e}{\partial x} + p_{b_f}\frac{\partial b}{\partial x} - \frac{1}{\alpha_f N_R}\left\{2\frac{\partial^2 u_f}{\partial x^2} - \frac{\chi u_f}{\varepsilon^2 h^2}\right\} + \frac{1}{\alpha_f N_{R_A}}\left\{2\frac{\partial}{\partial x}\left(\frac{\partial\alpha_s^e}{\partial x}\left(u_f - u_s\right)\right)\right\} \\ - \frac{\xi\alpha_s^e\left(u_f - u_s\right)}{\varepsilon^2\alpha_f N_{R_A} h^2}\Bigg]\Bigg] - \frac{1}{\gamma}C_{DG}\left(u_f - u_s\right)|u_f - u_s|^{j-1}. \end{aligned} \tag{6}$$

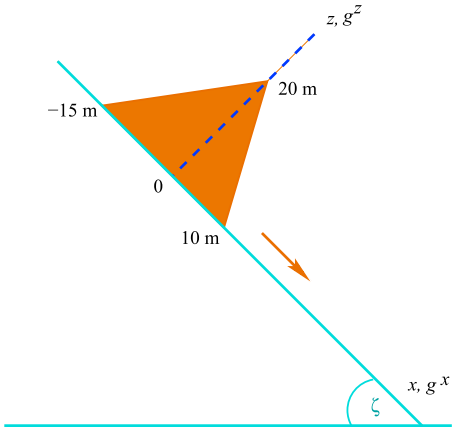

Figure 2. Geometry and initial setting for the two-phase rock-ice debris avalanche simulation. Initial material consists of a mixture of solid and fluid with effective initial solid volume fraction of about $\alpha_s^e = 0.75$.

The parameters are as follows:

$$\beta_s = \varepsilon K p_{b_s},\ \beta_f = \varepsilon p_{b_f},\ p_{b_f} = -g^z,\ p_{b_s} = (1-\gamma)p_{b_f},$$
$$C_{\mathrm{DG}} = \frac{\alpha_s^e \alpha_f (1-\gamma)}{\left[\varepsilon \mathcal{U}_T \{\mathcal{P}\mathcal{F}(Re_p) + (1-\mathcal{P})\mathcal{G}(Re_p)\}\right]^J},$$
$$\alpha_f = 1 - \alpha_s^e,\ \mathcal{F} = \frac{\gamma}{180}\left(\frac{\alpha_f}{\alpha_s^e}\right)^3 Re_p,\ \mathcal{G} = \alpha_f^{M(Re_p)-1},$$
$$\gamma = \frac{\rho_f}{\rho_r},\ Re_p = \frac{\rho_f d\, \mathcal{U}_T}{\eta_f},\ N_R = \frac{\sqrt{gL}H\rho_f}{\alpha_f \eta_f}, N_{R_{\mathcal{A}}} = \frac{\sqrt{gL}H\rho_f}{\mathcal{A}\eta_f}. \quad (7)$$

Here x and z are coordinates along and normal to the slope, and g^x and g^z are the components of gravitational acceleration (Figure 2). The solid and fluid constituents are denoted by the suffices s and f, respectively. The flow depth measured along z is denoted by h, u_s and u_f are the solid and the fluid velocities in the x direction, and $\mathcal{M}_p$ is the mass production for the fluid. The densities and volume fractions of the solid (rock) and the fluid are ρ_r, ρ_f, and α_s^e, α_f, respectively. L and H are the typical length and depth of the flow, and $\varepsilon = H/L$ is the aspect ratio. $K = K\left(\phi_s^e, \delta_s^e\right)$ is the earth pressure coefficient, C_{DG} is the generalized drag coefficient, $J = 1$ or 2 represents the simple linear or quadratic drag. $\mathcal{U}_T$ is the terminal velocity of a particle and $\mathcal{P} \in [0, 1]$. The factors p_{b_f} and p_{b_s} are associated with the effective fluid and solid pressures at the base. The density ratio is γ, C is the virtual mass coefficient (solid particle-induced kinetic energy of the fluid), η_f is the fluid viscosity, M is a function of the particle Reynolds number (Re_p), and χ and ξ represent the velocity and the solid volume fraction structure through the depth. $\mathcal{A}$ is the mobility of the fluid at the interface, and N_R and $N_{R_{\mathcal{A}}}$ are quasi-Reynolds numbers associated with the classical Newtonian and nonclassical non-Newtonian fluid viscous stresses, respectively. These numbers are manifestations of the dynamics of the fluid, in contrast to the mixture models [*Iverson and Denlinger*, 2001; *Pudasaini et al.*, 2005b] in which N_R is related to the dynamics of the debris bulk [*Pudasaini*, 2012, 2014; *Pudasaini and Miller*, 2012a, 2012b].

There are four important aspects of the model equations (3)–(7). (a) The right-hand sides of the mass balances in (3) are supplied with the mass loss in the solid ($-\mathcal{M}_p$) and the mass gain ($\mathcal{M}_p$) in the fluid, respectively. The momentum equations (4) are accordingly enhanced by introducing the momentum loss in solid and gain in fluid, $-\mathcal{M}_p u_s$ and $\mathcal{M}_p u_f/\gamma$, respectively, where, as in the drag term in the fluid momentum balance (6), the factor $1/\gamma$ appears due to scaling and can be called as the momentum amplifying factor. (b) The (inertial) terms on the left-hand side of (4) include the lateral pressures (associated with β_s and β_f) and the virtual mass, C. (c) The source in the solid momentum (5) have three different contributions: (i) gravity, the Coulomb friction, and the slope gradient (first square bracket); (ii) terms associated with the buoyancy force (second square bracket); and (iii) the generalized drag contributions $\left(C_{\mathrm{DG}}\right)$ (last term). The source term for the fluid momentum equation, (6), has six different contributions. The first three terms (on the right-hand side) emerge from the gravity load (first term), the term related to the fluid pressure gradient at the bed (second term), and the fluid pressure applied to the topographic gradient (third term), respectively. The fourth and fifth group of terms associated with N_R and $N_{R_{\mathcal{A}}}$ are the Newtonian viscous, and the solid volume fraction gradient-enhanced non-Newtonian viscous stresses, respectively. Finally, the last term represents the drag force. (d) As compared to the original debris flow model [*Pudasaini*, 2012], the model equations (3)–(7) are developed with some new effective field variables and parameters. This includes the effective solid volume fraction α_s^e, as a new field variable, the density ratio γ, which here is the ratio between the fluid and rock density, effective earth pressure coefficient K, which is now the function of the effective internal and basal friction angles and fluidization and lubrication factors. These variables and parameters explicitly and dynamically influence the following: (i) the mass and momentum productions (expressed in terms of $\mathcal{M}_p$ through the effective solid volume fraction and the fluidization velocity), (ii) the inertial terms in the (mass and) momentum equations, including the terms associated with the virtual mass contribution (that appears as a multiple of γ), (iii) the hydraulic pressure gradient (for solid β_s) via the effective earth pressure coefficient K and the buoyancy-reduced solid load as modeled by the factor $(1-\gamma)$, (iv) the net driving

force for the solid $\mathcal{S}_s$ is largely influenced by the effective solid volume fraction, the buoyancy-reduced solid load, and the density ratio in each terms including the gravity load, Coulomb friction, basal topographic effect, the term associated with the buoyancy, and the generalized drag term. (v) Similar analysis also holds for the net driving force for the fluid constituent, $\mathcal{S}_f$. (vi) Furthermore, the hydraulic pressure parameter (β_s), the normal load of solid at the bed (p_{b_s}), the generalized drag coefficient (C_{DG}), the fluid-like ($\mathcal{F}$) and solid-like ($\mathcal{G}$) drag contributions, the volume fraction of the fluid, and quasi-Reynolds numbers (N_R, N_{R_A}) are directly influenced, and they evolve as the functions of the above mentioned new effective variables and mechanical parameters. Thus, the presence of ice in rock-ice avalanches affects multiple processes and related physical terms in the new enhanced mechanical model for rock-ice avalanche via the mass and momentum balances.

3.4. Numerical Integration Technique

In rock avalanche simulations, the applied computational models are often only able to simulate smooth changes in flow variables [*Crosta et al.*, 2004; *Sosio et al.*, 2008; *Pirulli*, 2009]. However, the sudden jumps (shocks) and discontinuities are observed in the field and in laboratory flows of rock and sand avalanches and debris flows [*Pudasaini and Hutter*, 2007; *Pudasaini et al.*, 2007]. These phenomena are better captured by the high-resolution shock-capturing scheme. The model equations (3) and (4) are written in well-structured standard conservative form of hyperbolic-parabolic partial differential equations. This facilitates numerical integration even when shocks are formed in the field variables [*Pudasaini et al.*, 2005a, 2005b; *Takahashi*, 2007; *Pudasaini and Kroener*, 2008; *Pudasaini*, 2012]. Model equations are solved in conservative variables $\mathbf{W} = \left(h_s, h_f, m_s, m_f\right)^t$, where $h_s = \alpha_s^e h$, $h_f = \alpha_f h$ are the effective solid and the fluid contributions to the debris height and $m_s = \alpha_s^e h u_s$, $m_f = \alpha_f h u_f$ are the effective solid and fluid momentum fluxes, respectively [*Pudasaini and Miller*, 2012a, 2012b; *Pudasaini*, 2014]. We implement the high-resolution shock-capturing Total Variation Diminishing Non-Oscillatory Central (TVD-NOC) scheme [*Nessyahu and Tadmor*, 1990; *Tai et al.*, 2002; *Pudasaini et al.*, 2005a, 2005b; *Pudasaini and Hutter*, 2007; *Pudasaini*, 2012, 2014].

4. Simulations of Rock-Ice Avalanches

The original two-phase debris flow model, without ice effects, has been applied to simulate simple one-dimensional flows of debris mixture sliding down an inclined channel, submarine landslides, and induced tsunami [*Pudasaini*, 2012, 2014; *Pudasaini and Miller*, 2012a, 2012b]. Including the above mentioned ice-, snow-, and water-dependent mobility, lubrication, fluidization, effective friction parameters, and mass and momentum productions associated with the rock-ice avalanche, in this paper, we apply and numerically integrate the new general two-phase rock-ice debris avalanche model (3)–(7) to simple (benchmark) rock-ice avalanche simulations in order to describe these flows in a physically appropriate way. Although the mass and momentum exchanges between the sliding mass and the material boundary (e.g., the basal surface) are simulated in mass flows [*Hungr and Evans*, 2004; *Sovilla et al.*, 2006; *Pudasaini and Hutter*, 2007], internal mass and momentum exchanges between the phases is novel. In contrast to the usual debris flows and avalanches [*Savage and Hutter*, 1989; *Pitman and Le*, 2005], rock-ice-water debris flow is a unique situation in which there is a substantial mass and momentum exchange between the solid (ice) and the fluid (water or the slurry). Here we analyze in detail the influence of the effective internal and basal frictions, fluidization and lubrication factors, and internal mass and momentum exchanges between the phases on the overall dynamics.

4.1. Simulation Setup

We consider an inclined channel (slope, $\zeta = 45°$, Figure 2). The initial debris triangle is filled with 75% solid. Internal and basal friction angles of the solid phase are $\phi = 35°$ and $\delta = 25°$, respectively. Other parameter values are the following (also see *Pudasaini* [2012, 2014] and *Pudasaini and Miller* [2012a, 2012b]): $\rho_f = 1100$ kg m^{-3}, $\rho_r = 2900$ kg m^{-3}, $N_R = 600{,}000$, $N_{R_A} = 150{,}000$, $\mathcal{C} = 0$, $Re_p = 1$, $\mathcal{U}_T = 1$, $\mathcal{P} = 0.5$, $\mathcal{J} = 1$, $\chi = 3$, $\xi = 5$, $\lambda_\phi = 0.012$, $\lambda_\delta = 0.013$, and $M_{pf} = 0.018$, respectively. For the present simulation, the fluidization (similarly, liquefaction) factor is chosen as

$$F_\phi = \left[1 - \left(1 - \frac{\alpha_s^e - \alpha_{s_{\min}}^e}{\alpha_{s_{\max}}^e - \alpha_{s_{\min}}^e}\right)^\omega\right], \tag{8}$$

where $\omega = 2.0$ is the fluidization exponent (defining the shape of the fluidization) and $(\alpha_{s_{\min}}^e, \alpha_{s_{\max}}^e) = (0.05, 0.85)$ is set in simulation. The choice of this function is compatible to the observation of the laboratory

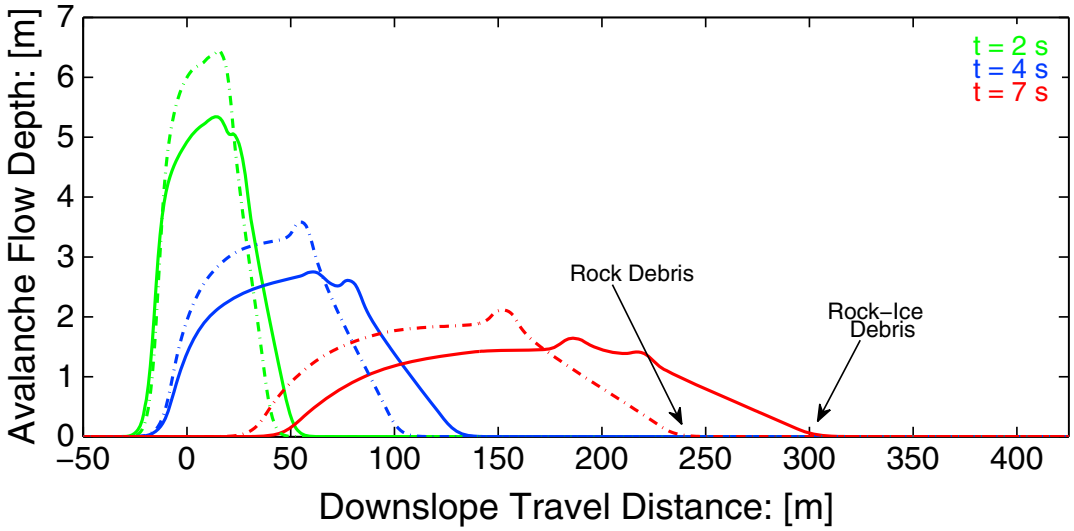

Figure 3. Rock debris and rock-ice debris evolve differently: the rock-ice debris (solid lines) moves faster than the rock debris (dash-dotted lines).

rock-ice avalanche by *Schneider et al.* [2011a] which showed that in the initial stages of the motion, the mixture behaves more like solid. As time evolves and the mass travels long downslope distance, the propagating rock-ice mass turns into debris mixture consisting of rock particles, ice fragments, and the melted fluid. Then, as soon as majority of ice is melted, the mixture quickly turns into fluid-dominated debris flow, and even hyperconcentrated flows. Such phenomena can be quantitatively described by (8).

4.2. Results and Discussions

For two-phase rock-ice avalanche simulations, we discuss here four different situations: rock debris avalanche, rock-ice debris avalanche, rock-ice debris avalanche with mass exchange, and rock-ice debris avalanche with mass and momentum exchanges.

1. *Rock Debris Avalanche.* The "rock debris avalanche" in which the internal and basal friction angles are constant, and there is no mass exchange has been presented in Figure 3 (dash-dotted lines).
2. *Rock-Ice Debris Avalanche.* The effective internal and basal friction angles of the solid (ϕ_s^e) and (δ_s^e) associated with internal fluidization and lubricating effects evolve as functions of the effective solid volume fraction (α_s^e). Simulation associated with this is called the "rock-ice debris avalanche" and is depicted in Figure 3 (solid lines).
   Figure 3 shows the substantial mobility of the rock-ice debris mass as compared to the same for the rock debris mass. Due to the ice-induced effective internal and basal friction angles of the solid ϕ_s^e and δ_s^e, and the associated internal fluidization and lubricating effects (F_ϕ and L_δ), the rock-ice debris (solid lines) has substantially less frictional strength, has greater degree of fluidization, and slides faster than the rock debris (dash-dotted lines) with the constant internal (ϕ_r) and the basal (δ_r) friction angles. In this simulation, mass exchange between the solid (i.e., ice) and the fluid is neglected. At $t = 2$, 4, and 7 s, the front of the rock debris and the rock-ice debris (rock debris, rock-ice debris) are at positions about (47 m, 57 m), (106 m, 135 m), and (238 m, 306 m), respectively. So the difference between the front positions of the rock debris and rock-ice debris at these times are about 10 m, 29 m, and 68 m, respectively. The front speeds for the rock debris and rock-ice debris are about (23, 26, 34) m s^{-1} and (28, 33, 43) m s^{-1} at times (2, 4, 7) s. Although these speeds may seem to be somewhat higher, nevertheless with respect to the amount of the total mass, travel distances, and the associated mechanisms for debris flows, subject to scrutiny, these numbers are reasonable.
3. *Rock-Ice Debris Avalanche With Internal Mass Exchange.* Another situation combines the evolving effective solid volume fraction in accordance with the mass exchange between the solid (ice) and the fluid and the corresponding effective solid internal and the basal friction angles, and associated internal fluidization and lubricating effects. Effective solid volume fraction is decreased with the mass exchange. Fluidization and lubrication decrease effective internal and basal friction angles (Figure 4). This is called the "rock-ice debris avalanche with mass exchange." Figure 4 shows that the dynamics of the rock-ice bulk material

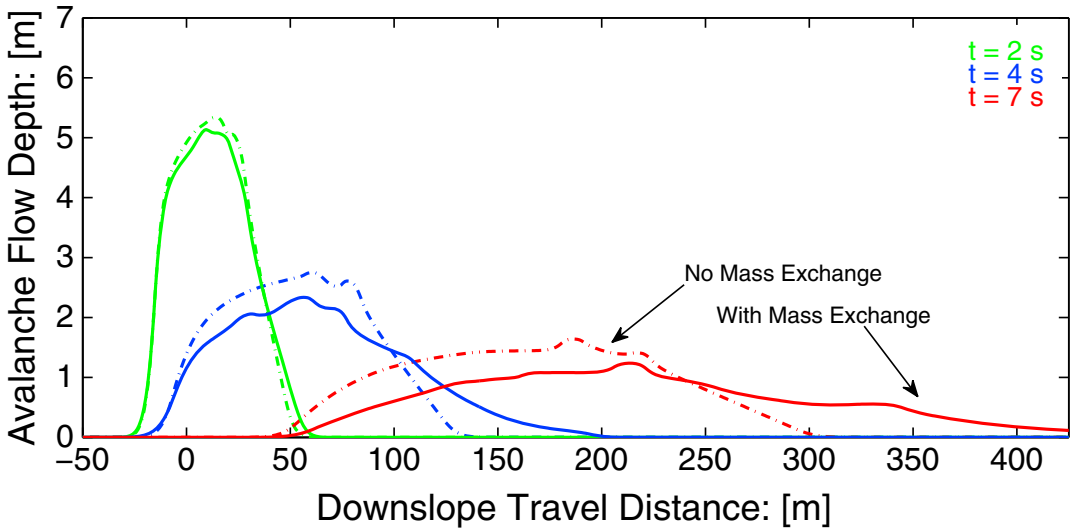

Figure 4. Deformation and motion of the rock-ice bulk debris material with (solid lines) and without (dash-dotted lines) the mass exchange are fundamentally different. The relative difference between the fronts of the debris avalanche with the mass exchange and the same without the mass exchange is rapidly increasing with time.

with (solid lines) and without (dash-dotted lines) the mass exchange are completely different. The relative progression of the fronts of the debris avalanche with the mass exchange and the same without the mass exchange is rapidly increasing with time. At $t = 7$ s, the difference is already about 119 m. The ice-related mass mobility is clearly demonstrated by comparing the front positions of the sliding debris with and without the mass exchange. The difference increases in time. At time $t = 7$ s, the front of the rock debris (Figure 3) is at $x = 238$ m, whereas the front of the rock-ice debris with mass exchange is at about $x = 425$ m, the difference is 187 m. At time $t = 2, 4$, and 7 s, the front positions of the bulk debris without mass exchange and mass exchange (no mass exchange, with mass exchange) are at about (57 m, 63 m), (134 m, 200 m), and (306 m, 425 m), respectively. So the distance between the front of the debris bulk without mass exchange and the debris bulk with mass exchange have been substantially increased from 6 m at $t = 2$ s to 66 m at $t = 4$ s to 119 m at $t = 7$ s, respectively.

4. *Rock-Ice Debris Avalanche With Internal Mass and Momentum Exchanges.* The most general scenario includes the ice-related effective internal and basal friction angles as functions of the effective solid volume fraction, fluidization and lubrication factors, and the mass and the momentum exchanges between the phases as shown in Figure 5. This is referred to as "rock-ice debris avalanche with mass and momentum exchanges". Simulation results with internal mass and momentum exchanges (solid lines) and without momentum exchange (dash-dotted lines) are shown in Figure 5. As time evolves, with the momentum exchange, the debris front is amplified and the debris mass thins in the tail side as observed in debris flow events and simulations (Bliggspitze event, 2007; Figure 1; [*Pudasaini et al.*, 2005b]). In these two situations (dash-dotted lines and solid lines), the debris evolutions are completely different. Both forms of the debris are observed in nature. So the observed forms of the evolving debris can be modeled by the internal momentum exchange between the phases. At time $t = 2, 4$, and 7 s, the front positions of the bulk debris without momentum exchange and with momentum exchange (no momentum exchange, with momentum exchange) are at about (61 m, 61 m), (200 m, 175 m), and (425 m, 406 m), respectively. So the distance between the front of the debris bulk without momentum exchange and with momentum exchange have been increased from 0 m at $t = 2$ s to 25 m at $t = 4$ s and about 20 m at $t = 7$ s, respectively. The front positions are much farther downslope as compared to the same in Figure 3. However, the differences between the front positions are much smaller as compared to the same in Figure 4, because here the momentum exchange has mainly resulted in the change of the flow front geometry rather than the front position. This can be physically explained as the internal momentum exchange pushes the mass from the back to the front.

   This is so because as the solid momentum is decreased and the fluid momentum is increased, less energy is dissipated in the back and/or tail side of the debris body that enhances the forward motion resulting in more mass accumulation in the front. Only with the mass exchange the front moves a bit

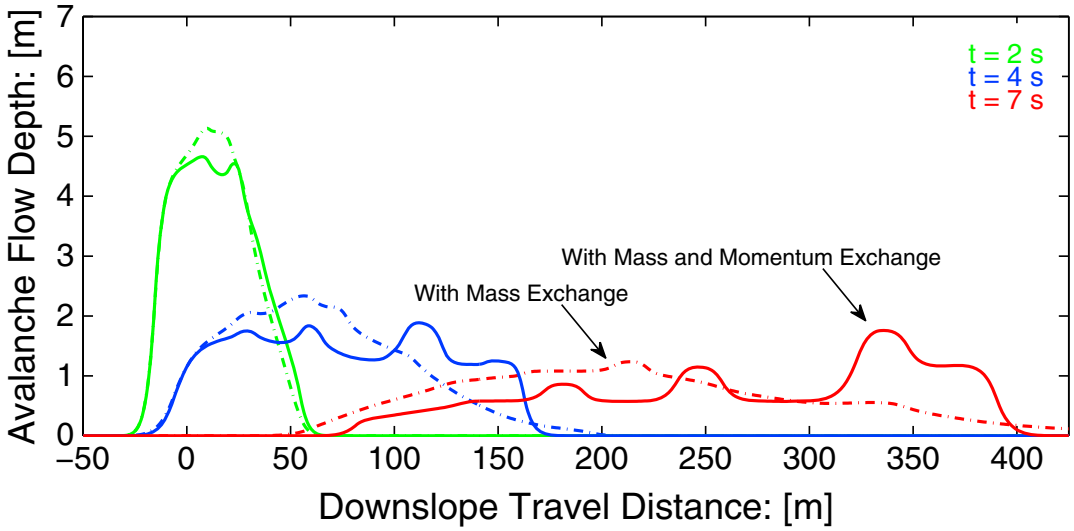

Figure 5. Same as Figure 4 (dash-dotted lines) but incorporating the internal momentum exchange between the phases (solid lines). As time evolves, with the momentum exchange, the debris front is amplified and the debris mass thins in the tail side. The debris evolutions are completely different with and without momentum exchanges.

unexpectedly long distance in an uncontrolled manner. However, mass exchange must be accompanied by the corresponding momentum exchange to have a physically meaningful and controlled simulation. When the momentum exchange is introduced, this controls the thin front (previously produced by applying only the mass exchange) and that more mass from the middle to the back becomes weaker, momentum of the fluid-like mass is increasing as modelled by the momentum production for the fluid phase, thus making the debris body mechanically weaker in the middle, back, and the tail, but at the same time, the relatively increased momentum production (for fluid) in the rear and middle part pushes additional debris mass to the front. This leads to the formation of the frontal surge head. Importantly, how the momentum exchange pushes the additional mass from the back to the front has clearly been demonstrated by comparing the differences in the tail positions, and the difference in mass (here area) in Figure 5 at time $t = 7$ s with (solid line) and without (dash-dotted line) momentum exchanges. This can also be discussed and justified in terms of the momentum losses and productions for the solid and the fluid (section 3.2). So the main mechanism for the mass accumulation and the surge development in the front is the transformation of the solid-like mass to the fluid-like mass and the associated internal momentum exchange.

Simulations in Figure 6 incorporate the momentum exchange between the phases (solid lines) and without momentum exchange (dash-dotted lines) but in both simulations with constant internal and basal friction angles, and there is no fluidization and lubrication effects. There are fundamental differences between Figures 5 and 6. On the one hand, in Figure 6, with and without momentum exchange, the front positions remain relatively close to each other. But the front positions in Figure 5 with fluidization and lubrication are much farther downslope as compared to the front positions in Figure 6 without fluidization and lubrication. So fluidization and lubrication are mainly responsible for the enhanced mobility (travel distance), and the internal mass and momentum exchanges result in the development and amplification of the frontal surge head and the thin and long tail in the rear of the cascading two-phase debris mass. On the other hand, for the solutions with momentum exchange, since the early stages (e.g., $t = 4$ s), the front has been less advanced but strongly sharpened in Figure 6 (constant internal and basal friction angles) than in Figure 5 (enhanced and variable internal and basal friction angles). This can be explained mechanically, because in Figure 6, internal and basal frictions remain strong as they are not evolving (not diminishing with effective solid volume fraction), and fluidization and lubrication do not take place. Then, as the mass is strong internally and along the base, higher frictions held the mass in the front creating a favorable condition for strong front amplifications with substantially hindered motion in Figure 6 than in Figure 5.

Figure 7 displays, for time $t = 7$ s, the effects of the changing friction angles and the internal and basal material weakening. In these simulations, mass and momentum exchanges are included. The dashed line

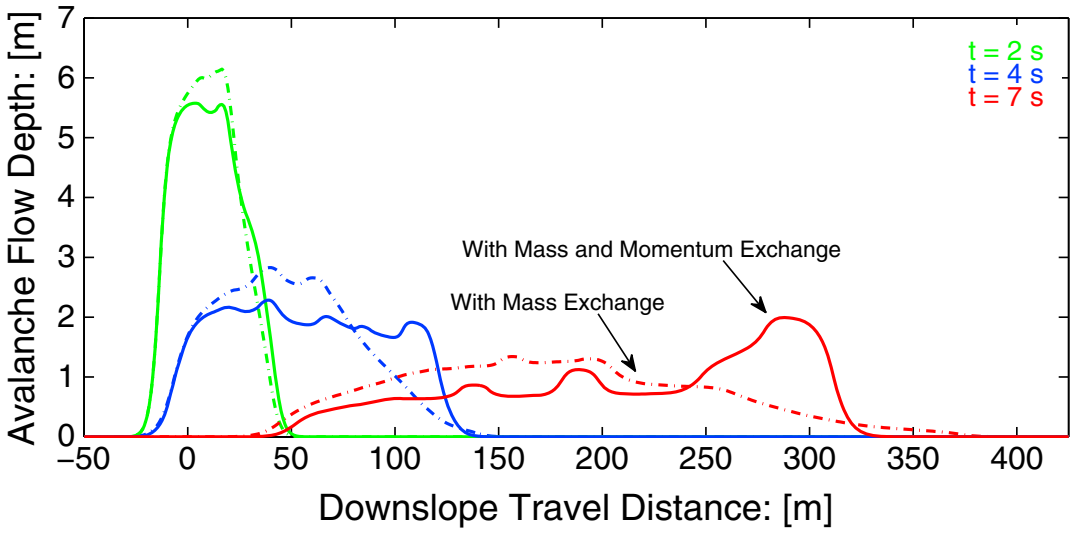

Figure 6. Same as Figure 5, but here the internal and basal frictions are constants, and there is no fluidization and lubrication effects. Here the front positions with (solid lines) and without (dash-dotted lines) momentum exchange remain close to each other, but the front positions in Figure 5 with fluidization and lubrication are much farther. The bulk mass here is much less mobile as compared to the same in Figure 5.

corresponds to the simulation with constant internal and basal friction angles and no internal fluidization and basal lubrication. The dash-dotted line is produced by using the variable friction angles but still without fluidization and lubrication. Due to the reduced frictions, in this simulation (dash-dotted line), the mass has advanced substantially in the downstream direction by about 30 m than in the previous simulation (dashed line). However, since the fluidization and lubrication effects are switched off, more mass accumulates in the front than in the previous case (dashed line). The solid line represents the simulation with variable frictions and including fluidization and lubrication effects. Due to the associated internal fluidization and lubrication, the previously largely amplified frontal surge (dash-dotted line) has now been stretched in the downstream in which the front advances farther by about 45 m resulting in the reduced frontal surge than in the previous situation. Mainly, the frontal geometries in these simulations are substantially different. The front positions, respectively, are at about 330, 360, and 406 m in the downstream. These simulations clearly demonstrate

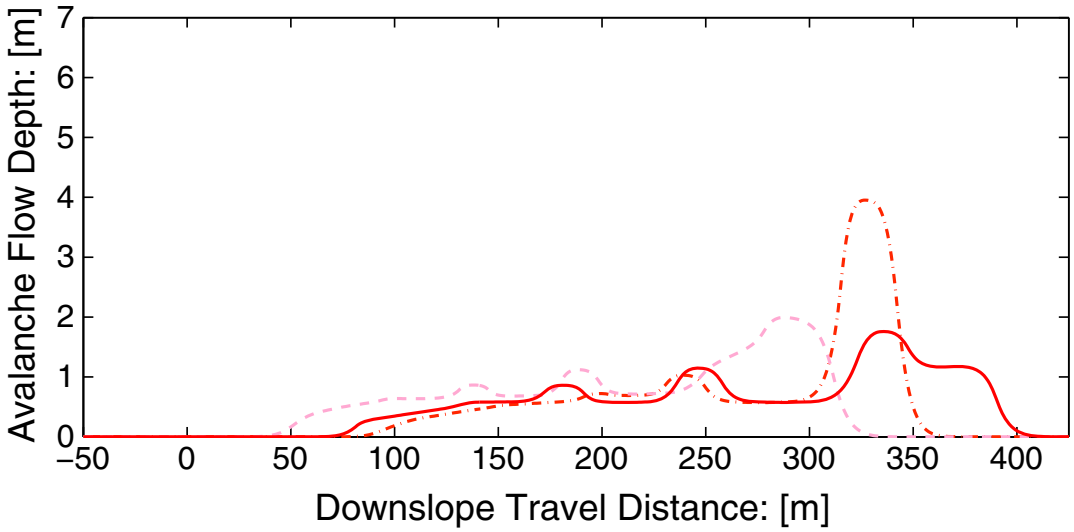

Figure 7. Showing the substantial effects of variable frictions, and fluidization and lubrication in determining the position and geometry of a two-phase rock-ice avalanche. The dashed, dash-dotted, and solid lines correspond, respectively, to the constant internal and basal frictions and no internal fluidization and basal lubrication, variable internal and basal frictions but no fluidization and lubrication, and variable frictions with fluidization and lubrication.

that the dynamically evolving internal and basal frictions and fluidization and lubrication factors play important role in determining the flow mobility and geometry of the cascading two-phase rock-ice debris mass. Most probably, the solid line represents the real flow scenario.

4.3. Implications

Many dynamically important and previously unreported observations are presented in the above figures. Three main mechanisms are responsible to decrease the material strength and thus enhance the mass mobility. Coincident to the internal mass and the momentum productions (from solid to fluid), the volume fraction of the solid and fluid changes, effective frictions, fluidization, and lubrication parameters will evolve. This controls the entire dynamics of the flow. This is a scenario in the rock-ice avalanche in which a large amount of the ice cover, glacier ice, and the internal ice may be converted into water during the flow, as observed in the rock-ice avalanches in Kolka-Karmadon (2002) and Bliggspitze (2007) and in the laboratory experiments [*Schneider et al.*, 2011a].

The generation, evolution, and downslope propagation of the rock-ice avalanche head is a characteristic for two-phase debris flows. Depending on the underlined mechanism, flow dynamics, topographic and boundary conditions, initial amount and the spatial temporal evolution of the solid and fluid components, the head may be fluid or solid rich [*Schneider et al.*, 2011a]. Higher mobility is associated with the fluid-rich head in contrast to the more resistive solid-rich head. With the internal mass and momentum exchanges, our model can reproduce both of these forms.

The front of the debris as simulated by using the new enhanced model that includes the internal fluidization and basal lubrication and the changing internal and basal friction angles together with the interphase mass and momentum exchanges (Figure 5) has proceeded much further than the front of the debris as simulated by using constant internal and basal friction angles, and neglecting the internal fluidization and basal lubrication (Figure 3). The difference is about 25%. This enhanced motion is in line with the inferences by *Bottino et al.* [2002] and the findings by *Sosio et al.* [2012]. Simulations show that the flow mobility and enhanced runout distances are due to the dynamically changing internal and basal friction angles and the dynamic fluidization and dynamic lubrication. Moreover, dynamic lubrication may dominate the process as we are applying the depth-averaged version of the two-phase models. Simulations also indicate that in short times, changes are very little both for the dynamic strength weakening and mass and momentum exchanges as seen in the experiments by *Schneider et al.* [2011a].

Mass and momentum exchanges may be less pronounced in the beginning of the mass collapse and in the early stages of the motion. These exchanges may cease after some time as the bulk have moved certain distance [*Schneider et al.*, 2011a]. This can be easily accounted for in our simulation by considering the mass and momentum exchange domain. Increasing this domain leads to big changes in the results. For the Sherman rock avalanche, *Sosio et al.* [2012] simulated a peak in flow thickness close to the detachment area during the early stages of propagation. This corresponds to the high rate of ice melting after certain time after the mass collapse, which then decreases quickly but also produces secondary surge of ice melting later on. Our results are in line with those findings.

The simulation results reveal fundamentally new features of the proposed model equations (3)–(7) over the classical models and highlight the basic physics associated with the contributions of the new mechanics typically associated with permafrost environments and the rock-ice avalanches. Change in internal and basal frictions, fluidization and lubrication, and mass and momentum exchanges between the phases are associated with the distinct physical aspects in a real two-phase rock-ice avalanches. As the appropriate modeling of the rock-ice avalanches is crucial, and as the runout areas and impact forces are strongly dependent on the model, rheological equations, and parameters, all these different mechanisms should be included to properly model the rock-ice avalanches. Moreover, iceberg tsunamis and glacier caviting tsunamis [*MacAyeal et al.*, 2009, 2011] are another important examples where our two-phase strength weakening and internal mass and momentum exchange models can be used to simulate these complex phenomena.

Our results qualitatively correspond well to laboratory and field observations. Nevertheless, it is out of the scope of this paper to conduct a detailed quantitative evaluation with observations. However, this—in addition to building applications of the model useful for practical applications—would be an important future research direction. With a physically based modeling of granular flows, *Mergili et al.* [2012] have shown how to implement a complex mass flow model with geographic information system (GIS) and with a novel

approach to evaluate and compare computational snow avalanche simulation; *Fischer* [2013] has shown how to evaluate parameter sensitivity in a systematic way. These approaches can be applied to validate the new model with data sets available in literature, including *Schneider et al.* [2011a].

4.4. Discussions on the Influence of Model Parameters and Variables

As collected in (7), there are several parameters in the model which are derived from a few measurable physical and geometrical parameters. Although this paper is mainly focused on presenting a new two-phase mechanical model for rock-ice avalanche and some basic benchmark simulations, we also performed several simulations with varied parameter values to have some ideas on the major effects of these parameters on the overall simulation results. Here only the qualitative discussion is presented for some important parameters. Nevertheless, which methods and parameter values are physically more meaningful must be tested against data, which, however, is not within the scope here.

Simulations were performed with the TVD-NOC method with Minmod limiter [*Pudasaini and Hutter*, 2007], with the Courant-Friedrichs-Lewy (CFL) number 0.05, and 501 grid points for the channel length of 475 m. However, the CFL number could be chosen differently, e.g., between 0.04 and 0.15 to produce the results as presented here. The van Leer limiter produced very amplified bore-type front surges. Weighted essentially nonoscillatory [see, e.g., *Pudasaini and Hutter*, 2007] method resulted in sharp front and several sharper secondary surges.

As in *Pudasaini* [2012], the results are obtained by employing the coupled and enhanced solid- and fluid-phase eigenvalues and phase wave speeds. Such coupled descriptions increase the flow mobility [*Pokhrel*, 2014] as the coupling enhances the phase wave speeds and momentum, e.g., via the hydraulic pressure gradient (for solid). Similarly, the drag for solid, hydraulic pressure gradient and wave speeds are also influenced by the effective density ratio (via buoyancy-reduced solid load), effective internal and basal friction angles, and effective earth pressure coefficients.

Mixture velocity (or the fluidization velocity) u_m, which appears in the internal mass and momentum productions ($\mathcal{M}_p$), plays an important role in generating the more amplified frontal surge head as presented above. If, instead, only the solid velocity (u_s) was used, which does not include the total velocity of the debris bulk, this would produce less amplified front head. Nevertheless, the central and the rear part of the debris remains effectively unchanged even with the use of u_s. Increasing the mass and momentum exchange factors (M_{pf}) results in highly amplified frontal surge and that the debris mass is pushed substantially in the downstream. These findings indicate that the appropriate modeling of the mass and momentum exchanges is essential in generating more meaningful and physically reasonable results.

Changing the quasi-Reynolds numbers N_R and N_{R_A} by an order of magnitude mainly results in the change in the frontal part of the flow. However, except for such detailed quantitative differences, the overall debris forms remain largely unaltered. Furthermore, there are no remarkable changes in the earlier stages of the flow (e.g., $t = 2$ s). So the numbers N_R and N_{R_A} should be suitably selected.

Another important aspect is the extent of the domain of mass and momentum exchanges. Simulation results presented here are produced by assuming that the mass and momentum exchanges take place in the subdomain [−50, 120] m. Simulations produced with mass and momentum production subdomains, with − 50 m to the left and 30, 50, 70, 90, and 100 and 150, 200 m to the right, show that the enlarged domains result in producing the more and more amplified fronts. Interestingly, until $t = 2$ s nothing changes, as it takes some time for the mass and momentum exchange to show their effects. However, for $t = 4$ s, the mass from the front left was pushed forward to form a bore-type front. Further, for $t = 7$ s, the fronts have successively been amplified with increased domain of mass and momentum exchanges, and at the same time, the tails are correspondingly thinning and stretching.

Changing the initial geometry, e.g., by stretching the rear and the front of the initial triangular form of the debris, the results remain qualitatively similar: producing the front surge, secondary surges, and long thin tails. Simulations were also performed by introducing the horizontal part in the channel, e.g., the inclined part until $x = 150$ m and then horizontal part. With the horizontal part, for $t = 7$ s, except in the inclined part, the mass moves much slower as compared with the simulation with entire inclined channel in which mass moves much faster and farther down the channel. Also, there are significant changes in the geometry in the front with the horizontal part. Because in the horizontal part, the gravity is reduced and the friction dominates the flow, this slows down the motion, and the mass is accumulated in the front.

The parameter P that appears in the generalized drag describes the more solid-like or more fluid-like behavior of the flow. Relatively smaller values of P, e.g., $P = 0.15, 0.25$, that represent the dilute flow, result in longer runout distances. However, relatively larger values, e.g., $P = 0.65, 0.85$, that correspond to dense flows, induce more drag, resulting in large geometric changes, mainly in the front, but with reduced runout distances.

An order of magnitude change in the particle Reynolds number Re_p leads to substantial changes in the geometry and some changes in the flow front. Furthermore, reducing the value of $\alpha^e_{s_{\max}}$ (e.g., to 0.55) that appears as the upper limit of the fluidization and lubrication factors (F_ϕ, L_δ), strongly amplifies the front that is pushed a bit back; otherwise, the main body and the tail remain largely unchanged. Similarly, increasing the value of $\alpha^e_{s_{\min}}$ (e.g., to 0.25) shows the opposite results. These behaviors are intuitively clear because increased values of F_ϕ and L_δ correspond to increased frictions that result in holding the debris mass in the front, slow down the motion, and thus favoring the frontal amplification. However, simulation results are less sensitive to χ, ξ than other parameters.

5. Conclusion

To describe the typical dynamics of rock-ice avalanches, here we proposed a new two-phase mechanical model that appropriately represents changing fractions of rock, ice, snow (solid), and water (fluid). The model explains the dynamic strength weakening, and internal mass and momentum exchanges between phases. With this enhancement, the general two-phase debris flow model proposed by *Pudasaini* [2012] can be applied to rock-ice avalanches. As the meltwater largely reduces the friction resulting in the flow transformations, this can be used in scenario generation aiming at model simulations for hazard assessment with regard to potentially dangerous alpine rock walls that may turn into rock-ice avalanches. Benchmark numerical simulations demonstrate that the dynamics of rock-ice avalanches are fundamentally different from rock avalanches. New results add substantial values in properly modeling the runout distances, impact energies, impact heights, and the related hazard mitigation in the avalanche-prone high mountain environments.

Here, based on observations, we proposed three mechanisms and corresponding mechanical models that result in enhanced mobility of the rock-ice avalanche. (i) As the ice and snow melts during the propagation, the material strength reduces due to the weakening of the internal and basal frictions leading to the internal fluidization and basal lubrication. (ii) The moving mass quickly transforms from initially solid-like single-phase rock avalanche into effectively a two-phase solid-fluid mixture debris flow. (iii) As the ice and snow contained in the moving mass melt, more and more solid (say, ice) mass transforms into fluid from the initially rock-ice material. This typically results in the internal mass and momentum productions and exchanges between the solid and fluid phases.

The newly developed rheological model describes the effective basal and internal friction angles in terms of the evolving effective solid volume fraction, and lubrication and fluidization factors that are functions of several physical parameters and mechanical/dynamical variables. This fundamentally influences the overall dynamics resulting in more rapid flows, large runout distances, distinct flow, and deposition morphology in comparison to dry rock avalanches. The laboratory and field observations clearly reveal changing flow properties of rock-ice avalanche from solid-like to fluid-like and thus largely showing the two-phase nature of the flow. The available models are not able to simulate these complex events with process transformations and interactions as they use effectively single-phase mass flow models. The large uncertainty in parameter selection demands for more sophisticated models that take into account the naturally two-phase nature of the flows which, rather than focusing on parameter fittings, offers a more mechanical model that uses physically measurable and dynamically changing values of these parameters. Such a physically more justified modeling approach has been presented.

The ice-related mass mobility is clearly demonstrated by comparing the fronts of the sliding mass. Fluidization and lubrication, and internal mass exchange are mainly responsible for the enhanced mobility. With the mass exchange, the front positions are much farther downslope as compared to the front positions without the mass exchange, and the relative difference between the fronts is rapidly increasing with time. The rock-ice debris shows the substantial mobility contrary to the same for the rock debris mass. Whereas the internal momentum exchange results in the development and amplification of the frontal surge head and the thin and long tail of the cascading two-phase debris mass. This has been physically explained. Higher mobility is associated with the fluid-rich head in contrast to the more resistive solid-rich head. Our model

can reproduce both of these forms, and the results are in line with the findings by *Schneider et al.* [2011a] and *Sosio et al.* [2012]. It appears that these two-phase models and benchmark simulations are more consistent with observations and have the capability to dynamically represent the changing nature of rock-ice avalanches over time.

Acknowledgments
This work and the first author were financially supported by the German Research Foundation (DFG) through the research project, PU 386/3-1: *Development of a GIS-based Open Source Simulation Tool for Modelling General Avalanche and Debris Flows over Natural Topography* within a transnational research project, D-A-CH. We thank the three anonymous reviewers, and the Editor Bryn Hubbard for their constructive comments that helped to improve the manuscript significantly.

References

Armento, M. C., R. Genevois, and P. R. Tecca (2008), Comparison of numerical models of two debris flows in the Cortina d'Ampezzo area, Dolomites, Italy, *Landslides*, *5*, 143–150.
Bartelt, P., O. Buser, and K. Platzer (2006), Fluctuation-dissipation relations for granular snow avalanches, *J. Glaciol.*, *52*(179), 631–643.
Bartelt, P., Y. Bühler, O. Buser, M. Christen, and L. Meier (2012), Modeling mass-dependent flow regime transitions to predict the stopping and depositional behavior of snow avalanches, *J. Geophys. Res.*, *117*, F01015, doi:10.1029/2010JF001957.
Bottino, G., M. Chiarle, A. Joly, and G. Mortara (2002), Modelling rock avalanches and their relation to permafrost degradation in glacial environments, *Permafrost Periglac. Processes*, *13*, 283–288.
Chen, H., and C. F. Lee (2000), Numerical simulation of debris flows, *Can. Geotech. J.*, *37*, 146–160.
Chen, H., G. B. Crosta, and C. F. Lee (2006), Erosional effects on runout of fast landslides, debris flows and avalanches: A numerical investigation, *Geotechnology*, *56*(5), 305–322.
Crosta, G. B., H. Chen, and C. F. Lee (2004), Replay of the 1987 Val Pola Landslide, Italian Alps, *Geomorphology*, *60*(1–2), 127–146.
Crosta, G. B., H. Chen, and P. Frattini (2006), Forecasting hazard scenarios and implications for the evaluation of countermeasure efficiency for large debris avalanches, *Eng. Geol.*, *83*, 236–253.
Davies, T. R. H., and M. J. McSaveney (1999), Runout of dry granular avalanches, *Can. Geotech. J.*, *36*, 313—320.
Davies, T. R. H., M. J. McSaveney, and K. Kelfoun (2010), Runout of the Socompa volcanic debris avalanche, Chile: A mechanical explanation for low basal shear resistance, *Bull. Volcanol.*, *72*, 933–944.
De Blasio, F. V., and A. Elverhøi (2008), A model for frictional melt production beneath large rock avalanches, *J. Geophys. Res.*, *113*, F02014, doi:10.1029/2007JF000867.
Deline, P. (2001), Recent Brenva rock avalanches (Valley of Aosta): New chapter in an old story?, *Geogr. Fis. Din. Quat.*, *5*, 55–63.
Denlinger, R. P., and R. M. Iverson (2001), Flow of variably fluidized granular masses across three-dimensional terrain: 2. Numerical predictions and experimental tests, *J. Geophys. Res.*, *106*(B1), 553–566.
Denlinger, R. P., and R. M. Iverson (2004), Granular avalanches across irregular three-dimensional terrain: 1. Theory and computation, *J. Geophys. Res.*, *109*, F01014, doi:10.1029/2003JF000085.
Draebing, D., and M. Krautblatter (2012), P-wave velocity changes in freezing hard low-porosity rocks: A laboratory-based time-average model, *Cryosphere*, *6*, 1163–1174.
Dramis, F., M. Govi, M. Guglielmin, and G. Mortara (1995), Mountain permafrost and slope instability in the Italian Alps: The Val Pola landslide, *Permafrost Periglac. Processes*, *6*, 73–81.
Erismann, T. H. (1979), Mechanisms of large landslides, *Rock Mech.*, *12*, 15–46.
Erismann, T. H., and G. Abele (2001), *Dynamics of Rockslides and Rockfall*, Springer, New York.
Evans, S. G. (2006), Single-event landslides resulting from massive rock slope failure: Characterizing their frequency and impact on society, in *Landslides From Massive Rock Slope Failure*, edited by S. G. Evans et al., pp. 53-73, Springer, Dordrecht, Netherlands.
Evans, S. G., and J. J. Clague (1988), Catastrophic rock avalanches in glacial environments, in *Proc. 5th Int. Symposium on Landslides, 11–15 July, Lausanne, Switzerland*, edited by C. Bonnard, pp. 1153–1158, Balkema, Lausanne, Rotterdam, Netherlands.
Evans, S. G., and J. J. Clague (1998), Rock avalanche from Mount Munday, Waddington Range, British Columbia, Canada, *Landslide News*, *11*, 23–25.
Evans, S. G., N. F. Bishop, L. F. Smoll, P. Valderrama Murillo, K. B. Delaney, and A. Oliver-Smith (2009a), A re-examination of the mechanism and human impact of catastrophic mass flows originating on Nevado Huascaran, Cordillera Blanca, Peru in 1962 and 1970, *Eng. Geol.*, *108*(1–2), 96–118.
Evans, S. G., O. V. Tutubalina, V. N. Drobyshev, S. S. Chernomorets, S. McDougall, D. Petrakov, and O. Hungr (2009b), Catastrophic detachment and high-velocity long runout flow of Kolka Glacier, Caucasus Mountains, Russia in 2002, *Geomorphology*, *105*, 314–321.
Fischer, J.-T. (2013), A novel approach to evaluate and compare computational snow avalanche simulation, *Nat. Hazards Earth Syst. Sci.*, *13*, 1655–1667, doi:10.5194/nhess-13-1655-2013.
Fischer, J.-T., J. Kowalski, and S. P. Pudasaini (2012), Topographic curvature effects in applied avalanche modeling, *Cold Regions Science and Technology*, *74-75*, 21–30.
Geertsema, M., J. J. Clague, J. Schwab, and S. G. Evans (2006), An overview of recent large catastrophic landslides in northern British Columbia, *Eng. Geol.*, *83*, 120–143.
Giani, G. P., S. Silvano, and G. Zanon (2001), Avalanche of 18 January 1997 on Brenva glacier, Mont Blanc Group, Western Italian Alps: An unusual process of formation, *Ann. Glaciol.*, *32*(1), 333–338.
Govi, M. (1989), The 1987 landslide on Mount Zandila in the Val-tellina, Northern Italy, *Landslide News*, *3*, 1–3.
Gruber, S., and W. Haeberli (2007), Permafrost in steep bedrock slopes and its temperature-related destabilization following climate change, *J. Geophys. Res.*, *112*, F02S18, doi:10.1029/2006JF000547.
Gruber, S., M. Hoelzle, and W. Haeberli (2004), Permafrost thaw and destabilization of Alpine rock walls in the hot summer of 2003, *Geophys. Res. Lett.*, *31*, L13504, doi:10.1029/2004GL020051.
Haeberli, W., M. Wegmann, and D. Vonder Muhll (1997), Slope stability problems related to glacier shrinkage and permafrost degradation in the Alps, *Eclogae Geol. Helv.*, *90*, 407–414.
Haeberli, W., C. Huggel, A. Kääb, S. Zgraggen-Oswald, A. Polkvoj, I. Galushkin, I. Zotikov, and N. Osokin (2004), The Kolka-Karmadon rock/ice slide of 20 September 2002: An extraordinary event of historical dimensions in North Ossetia, Russian Caucasus, *J. Glaciol.*, *50*(171), 533–546.
Hewitt, K. (1999), Quaternary moraines vs catastrophic rock avalanches in the Karakoram Himalaya, Northern Pakistan, *Quat. Res.*, *51*(3), 220–237.
Hewitt, K., J. J. Clague, and J. F. Orwin (2008), Legacies of catastrophic rock slope failures in mountain landscapes, *Earth Sci. Rev.*, *87*, 1–38.
Huber, V. A. (1992), Der-Val-pola rockslide in the upper Valtellina valley of 28 July 1987, *Eclogae Geol. Helv.*, *85*, 307–325.
Huggel, C. (2009), Recent extreme slope failures in glacial environments: Effects of thermal perturbation, *Quat. Sci. Rev.*, *28*(11–12), 1119–1130.

Huggel, C., S. Zgraggen-Oswald, W. Haeberli, A. Kaab, A. Polkvoj, I. Galushkin, and S. Evans (2005), The 2002 rock/ice avalanche at Kolka/Karmadon, Russian Caucasus: Assessment of extraordinary avalanche formation and mobility, and application of QuickBird satellite imagery, *Nat. Hazards Earth Sys. Sci.*, *5*(2), 173–187.

Huggel, C., J. Caplan-Auerbach, C. F. Waythomas, and R. L. Wessels (2007), Monitoring and modeling ice-rock avalanches from ice-capped volcanoes: A case study of frequent large avalanches on Iliamna Volcano, Alaska, *J. Volcanol. Geotherm. Res.*, *168*(1–4), 114–136.

Huggel, C., S. Gruber, J. Caplan-Auerbach, R. L. Wessels, and B. F. Molnia (2008), The 2005 Mt. Steller, Alaska, rock-ice avalanche: What does it tell us about large slope failures in cold permafrost?, in *Proceedings of the Ninth International Conference on Permafrost, Fairbanks, Alaska, 29 June–3 July 2008*, vol. 1, edited by D. L. Kane and K. M. Hinkel, pp. 747-752, Univ. of Alaska Fairbanks, Fairbanks, Alaska.

Hungr, O. (2004), Landslide hazard assessment—Goals and challenges, *Innov. Mag.*, *8*, 12–15.

Hungr, O., and S. G. Evans (1996), Rock avalanche runout prediction using a dynamic model, in *Proceedings of the 7th International Symposium on Landslides, Trondheim, Norway, 17–21 June 1996*, vol. 1, edited by K. Senneset, pp. 223–238, Balkema, Rotterdamn, Netherlands.

Hungr, O., and S. G. Evans (2004), Entrainment of debris in rock avalanches: An analysis of a long run-out mechanism, *Geol. Soc. Am. Bull.*, *116*(9/10), 1240–1252.

Iverson, R. M., and R. P. Denlinger (2001), Flow of variably fluidized granular masses across three-dimensional terrain: 1. Coulomb mixture theory, *J. Geophys. Res.*, *106*(B1), 537–552, doi:10.1029/2000JB900329.

Kääb, A., et al. (2005), Remote sensing of glacier and permafrost related hazards in high mountains: An overview, *Nat. Hazards Earth Syst. Sci.*, *5*, 527–554.

Kotlyakov, V. M., O. V. Rototaeva, and G. A. Nosenko (2004), The September 2002 Kolka glacier catastrophe in North Ossetia, Russian Federation: Evidence and analysis, *Mt. Res. Dev.*, *24*(1), 78–83.

Körner, H. J. (1983), Zur Mechanik der Bergsturzströme vom Huascaran, Peru, in *Die Berg- und Gletscherstürze vom Huascaran, Cordillera Blanca, Per*, edited by G. Patzelt, pp. 71–110, Wagner Univ. Press, Innsbruck, Austria.

Korup, O. (2005), Large landslides and their effect on sediment flux in South Westland, New Zealand, *Earth Surf. Processes Landforms*, *30*, 305–323.

Krautblatter, M., D. Funk, and F. K. Günzel (2013), Why permafrost rocks become unstable: A rock-ice-mechanical model in time and space, *Earth Surf. Processes Landforms*, *38*, 876–887.

Legros, F., M. Cantagrel, and D. Bertrand (2000), Pseudotachylyte (frictionite) at the base of the Arequipa volcanic landslide deposit (Peru): Implications for emplacement mechanisms, *J. Geol.*, *108*, 601–611.

Lipovsky, P. S., et al. (2008), The July 2007 rock and ice avalanches at Mount Steele, St. Elias Mountains, Yukon, Canada, *Landslides*, *5*(4), 445–455.

MacAyeal, D. R., E. A. Okal, R. C. Aster, and J. N. Bassis (2009), Seismic observations of glaciogenic ocean waves (micro-tsunamis) on icebergs and ice shelves, *J. Glaciol.*, *55*(190), 193–206.

MacAyeal, D. R., D. S. Abbot, and O. V. Sergienko (2011), Iceberg-capsize tsunamigenesis, *Annal. Glaciol.*, *52*(58), 51–56.

Major, J., and R. M. Iverson (1999), Debris-flow deposition: Effects of pore-fluid pressure and friction concentrated at flow margins, *Geol. Soc. Am. Bull.*, *110*, 1424–1434.

Marangunic, C., and C. Bull (1968), The landslide on the Sherman Glacier, in *The Great Alaska Earthquake of 1964: Hydrology*, pp. 383–394, Natl. Acad. Sci. Publ. 1603, Washington, D. C.

Margreth, S., and M. Funk (1999), Hazard mapping for ice and combined snow/ice avalanches—Two case studies from the Swiss and Italian Alps, *Cold Reg. Sci. Technol.*, *30*(1-3), 159–173.

McArdell, B. W., P. Bartelt, and J. Kowalski (2007), Field observations of basal forces and fluid pore pressure in a debris flow, *Geophys. Res. Lett.*, *34*, L07406, doi:10.1029/2006GL029183.

McDougall, S., and O. Hungr (2004), A model for the analysis of rapid landslide motion across three-dimensional terrain, *Can. Geotech. J.*, *41*, 1084–1097.

McSaveney, M. J. (1978), Sherman glacier rock avalanche, Alaska, USA, in *Rockslides and Avalanches, Natural Phenomena*, edited by B. Voight, pp. 197–258, Elsevier, Amsterdam.

McSaveney, M. J. (2002), Recent rockfalls and rock avalanches in Mount Cook National Park, New Zealand, in *Catastrophic Landslides: Occurrence, Mechanisms and Mobility*, vol. 15, edited by S. G. Evans and J. V. DeGraff, pp. 35–70, Geol. Soc. Am. Rev. in Eng. Geol., Boulder, Colo.

McSaveney, M. J., and T. R. H. Davies (2006), Rapid rock mass flow with dynamic fragmentation: Inferences from the morphology and internal structure of rockslides and rock avalanches, in *Landslides From Massive Rock Slope Failure. Nato Science Series IV*, vol. 49, edited by S. G. Evans et al., pp. 285–304, Springer, Dordrent, Netherlands.

McSaveney, M. J., and T. R. H. Davies (2007), Rockslides and their motion, in *Progress in Landslide Science*, edited by K. Sassa et al., pp. 113–133, Springer, Berlin.

Mergili, M., K. Schratz, A. Ostermann, and W. Fellin (2012), Physically-based modelling of granular flows with Open Source GIS, *Nat. Hazards Earth Syst. Sci.*, *12*, 187–200.

Nessyahu, H., and E. Tadmor (1990), Non-oscillatory central differencing for hyperbolic conservation laws, *J. Comput. Phys.*, *87*, 408–463.

Petrakov, D. A., S. S. Chernomorets, S. G. Evans, and O. V. Tutubalina (2008), Catastrophic glacial multi-phase mass movements: A special type of glacial hazard, *Adv. Geosci.*, *14*, 211–218.

Pierson, T. C., and K. M. Scott (1985), Downstream dilution of a lahar: Transition from debris-flow to hyperconcentrated streamflow, *Water Resour. Res.*, *21*(10), 1511–1524.

Pirulli, M. (2009), The Thurwieser rock avalanche (Italian Alps): Description and dynamic analysis, *Eng. Geol.*, *109*, 80–92.

Pirulli, M., and G. Sorbino (2008), Assessing potential debris flow runout: A comparison of two simulation models, *Nat. Hazards Earth Syst. Sci.*, *8*, 961–971.

Pitman, E. B., and L. Le (2005), A two-fluid model for avalanche and debris flows, *Philos. Trans. R. Soc. A*, *363*, 1573–1602.

Plafker, G., and G. E. Ericksen (1978), Nevados Huascaran avalanches, Peru, in *Rockslides and Avalanches. 1: Natural Phenomena*, edited by B. Voight, pp. 277–314, Elsevier, Amsterdam.

Pokhrel, P. R. (2014), General phase-eigenvalues for two-phase mass flows: Supercritical and subcritical states, M. Phil. dissertation, Kathmandu Univ., School of Science, Kavre, Dhulikhel, Nepal.

Pudasaini, S. P. (2012), A general two-phase debris flow model, *J. Geophys. Res.*, *117*, F03010, doi:10.1029/2011JF002186.

Pudasaini, S. P. (2014), Dynamics of submarine debris flow and tsunami, *Acta Mech.*, *225*, 2423–2434, doi:10.1007/s00707-014-1126-0.

Pudasaini, S. P., and K. Hutter (2003), Rapid shear flows of dry granular masses down curved and twisted channels, *J. Fluid Mech.*, *495*, 193–208.

Pudasaini, S. P., and K. Hutter (2007), *Avalanche Dynamics: Dynamics of Rapid Flows of Dense Granular Avalanches*, 602 pp., Springer, New York.
Pudasaini, S. P., and C. Kroener (2008), Shock waves in rapid flows of dense granular materials: Theoretical predictions and experimental results, *Phys. Rev. E*, *78*(4), 041308, doi:10.1103/PhysRevE.78.041308.
Pudasaini, S. P., and S. A. Miller (2012a), Buoyancy induced mobility in two-phase debris flow, *AIP Conf. Proc.*, *1479*, 149–152.
Pudasaini, S. P., and S. A. Miller (2012b), A real two-phase submarine debris flow and tsunami, *AIP Conf. Proc.*, *1479*, 197–200.
Pudasaini, S. P., and S. A. Miller (2013), The hypermobility of huge landslides and avalanches, *Eng. Geol.*, *157*, 124–132.
Pudasaini, S. P., Y. Wang, and K. Hutter (2005a), Rapid motions of free-surface avalanches down curved and twisted channels and their numerical simulation, *Philos. Trans. R. Soc. A*, *363*(1832), 1551–1571.
Pudasaini, S. P., Y. Wang, and K. Hutter (2005b), Modelling debris flows down general channels, *Nat. Hazards Earth Syst. Sci.*, *5*, 799–819.
Pudasaini, S. P., K. Hutter, S.-S. Hsiau, S.-C. Tai, Y. Wang, and R. Katzenbach (2007), Rapid flow of dry granular materials down inclined chutes impinging on rigid walls, *Phys. Fluids*, *19*(5), 053302, doi:10.1063/1.2726885.
Ravanel, L., and P. Deline (2011), Climate influence on rockfalls in high-Alpine steep rockwalls: The north side of the Aiguilles de Chamonix (Mont Blanc massif) since the end of the 'Little Ice Age', *Holocene*, *21*, 357–365.
Savage, S. B., and K. Hutter (1989), The motion of a finite mass of granular material down a rough incline, *J. Fluid Mech.*, *199*, 177–215.
Schiermeier, Q. (2003), Alpine thaw breaks ice over permafrost's role, *Nature*, *424*, 712.
Schneider, D., P. Bartelt, J. Caplan-Auerbach, M. Christen, C. Huggel, and B. W. McArdell (2010), Insights into rock-ice avalanche dynamics by combined analysis of seismic recordings and a numerical avalanche model, *J. Geophys. Res.*, *115*, F04026, doi:10.1029/2010JF001734.
Schneider, D., C. Huggel, W. Haeberli, and R. Kaitna (2011a), Unraveling driving factors for large rock-ice avalanche mobility, *Earth Surf. Processes Landforms*, *36*(14), 1948–1966.
Schneider, D., R. Kaitna, W. E. Dietrich, L. Hsu, C. Huggel, and B. McArdell (2011b), Frictional behavior of granular gravel-ice mixtures in vertically rotating drum experiments and implications for rock-ice avalanches, *Cold Reg. Sci. Technol.*, *69*(1), 70–90.
Schneider, J. F. (2006), Risk assessment of remote geohazards in Western Pamir, GBAO, Tajikistan, in *Proceedings of the International Conference on High Mountaing Hazard Prevention, Vladikavkaz-Moscow, June 23–26, 2004*, pp. 252-267, Swiss Agency for Dev. and Coop., Vladikavkaz, Russia.
Sosio, R., G. B. Crosta, and O. Hungr (2008), Complete dynamic modeling calibration for the Thurwieser rock avalanche (Italian Central Alps), *Eng. Geol.*, *100*, 11–26.
Sosio, R., G. B. Crosta, J. H. Chen, and O. Hungr (2012), Modelling rock avalanche propagation onto glaciers, *Quat. Sci. Rev.*, *47*, 23–40.
Sovilla, B., P. Burlando, and P. Bartelt (2006), Field experiments and numerical modeling of mass entrainment in snow avalanches, *J. Geophys. Res.*, *111*, F03007, doi:10.1029/2005JF000391.
Strom, A. L., and O. Korup (2006), Extremely large rockslides and rock avalanches in the Tien Shan Mountains, Kyrgyzstan, *Landslides*, *3*, 125–136.
Surinach, E., F. Sabot, G. Furdada, and J. M. Vilaplana (2000), Study of seismic signals of artificially released snow avalanches for monitoring purposes, *Phys. Chem. Earth*, *25*(9), 721–727.
Tai, Y. C., S. Noelle, J. M. N. T. Gray, and K. Hutter (2002), Shock-capturing and front tracking methods for granular avalanches, *J. Comput. Phys.*, *175*, 269–301.
Takahashi, T. (2007), *Debris Flow: Mechanics, Prediction and Countermeasures*, Taylor and Francis, Leiden, Netherlands.
Voellmy, A. (1955), Über die Zerstörungskraft von Lawinen, *Schwerizerische Bauzeitung, Jahrgang*, *73*(12), 159–162.